Riemannian Metrics on the Space of Solid Shapes

P. Thomas Fletcher and Ross T. Whitaker

School of Computing
University of Utah
fletcher@sci.utah.edu, whitaker@cs.utah.edu

Abstract. We present a new framework for multidimensional shape analysis. The proposed framework represents solid objects as points on an infinite-dimensional Riemannian manifold and distances between objects as minimal length geodesic paths. Intershape distance forms the foundation for shape-based statistical analysis. The proposed method incorporates a metric that naturally prevents self-intersections of object boundaries and thus produces a well-defined interior and exterior along every geodesic path. This paper presents an implementation of the geodesic computations for 2D shapes and gives examples of geodesic paths that demonstrate the advantages of enforcing well-defined boundaries. This compares favorably with equivalent paths under a linear L^2 metric, which do not prevent self-intersection of the boundary, and thus do not produce valid solid objects.

1 Introduction

Shape analysis plays an important role in the understanding of anatomical variability from medical images. Statistics of shape is vital to applications ranging from disease diagnosis, treatment planning, and quantification of the effects of disease. While anatomy consists entirely of solid objects, many shape representations, such as landmarks, boundary curves, or harmonics, do not account for the solid nature of objects. In this paper we present a new shape metric that is well-suited to quantify shape changes in solid objects. We also show that representing shapes as solids results in a shape space that conforms qualitatively with some of our most natural intuitions about shape variabilities.

Quantitative study of shape begins with the formulation of a *shape space*, in which each shape is represented as a point. A distance metric on this shape space gives a measure of shape similarity between any two objects. When the shape space has the structure of a Riemannian manifold, this distance is given by minimal geodesics, or shortest length curve segments, between two shapes. The ability to compute distances between shapes is the foundation for statistical analysis. The first formulations of shape spaces, and the use of metrics to define shape statistics, were developed in the seminal works of Kendall [1] and Bookstein [2]. In their work a 2D object is represented as a discrete set of landmark points. By removing the effects of translations, rotations, and scalings of

these landmarks, the shape space is given the structure of a curved Riemannian manifold. The structure of this space can then be used to define probability distributions as in Mardia and Dryden [3]. The theory of landmark-based shape spaces is reviewed in several books [4], [5].

A typical strategy in shape analysis applications is to apply a linear metric on the parameters of the shape representation. The Active Shape Model (ASM) of Cootes and Taylor [6] represents objects as a dense sampling of their boundaries. They align objects using a Procrustes algorithm and perform principal components analysis (PCA) to capture the shape variability. Kelemen et al. [7] represent 3D objects by spherical harmonic (SPHARM) decompositions of their boundaries and quantify shape variation using PCA with a linear metric on the SPHARM coefficients. Shape variations under these metrics are characterized by straight line paths of object boundaries. Such deformations do not respect the solid properties of objects, and can create intersecting boundaries. Fletcher et al. [8] introduce a generalization of PCA to nonlinear manifolds and use it to compute shape statistics based on medial representations of objects. While nonlinear variations of shape provide a richer set of deformations, there is still no guarantee that shape boundaries will not intersect.

Recent work has focused on representing shape variations of continuous planar curves, where the shape spaces are infinite-dimensional manifolds. Klassen et al. [9] develop elastic curves based on an angle function of the tangent vector. Sharon and Mumford [10] design a metric based on conformal mappings between 2D objects. Michor and Mumford [11] investigate metrics on the space of smooth curves modulo reparameterizations. While this work lays a rigorous mathematical framework for comparing smooth curves, again there is no constraint that the curves not intersect. One method of shape analysis that does indeed constrain solid objects to be free of self-intersections is the diffeomorphic approach, first proposed by Grenander [12]. In this framework shape variations are represented as the actions of diffeomorphisms on a template. Miller and Younes [13] take this approach and define metrics on spaces of diffeomorphism groups, which are infinite-dimensional. While the diffeomorphism approach does preserve solid shapes, the metric is not defined directly on the shapes themselves. Rather, the metric is defined on the diffeomorphism group, which is combined with a matching term to deform one object into another.

In this paper we present a new shape representation which directly models solid objects. The shape space is an infinite-dimensional Riemannian manifold, with a metric designed to preserve non-intersecting boundaries of solid objects. Our framework is valid for objects in both 2D and 3D. The rest of this paper is organized as follows. In Section 2 we formulate the space of solid objects. We develop a Riemannian metric on this space in Section 3 and give a procedure to compute geodesics in Section 4. We present examples of these geodesics for 2D objects in Section 5 and demonstrate that they preserve non-intersecting object boundaries. We compare these geodesics to the equivalent minimal paths under a linear metric, which result in intersecting boundaries.

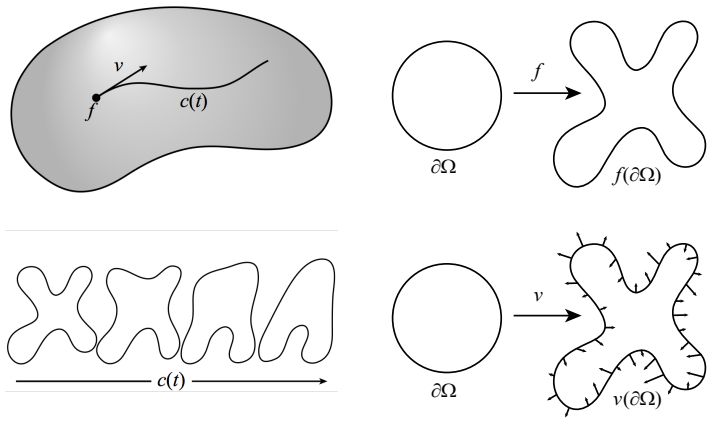

Fig. 1. A pictorial representation of the infinite-dimensional space of solid objects, $\mathcal{E}(\partial\Omega, \mathbb{R}^n)$ (top left). A point f in this space is an embedding representing a solid object (top right). A path $c(t)$ in this space is a smooth deformation of shapes (bottom left). A tangent vector v at the point f is a vector field on the image $f(\partial\Omega)$ that represents an infinitesimal deformation of f (bottom right).

2 The Space of Solid Objects

The proposed formulation of the space of solid objects relies on a fixed template object, which is a compact region $\Omega \subset \mathbb{R}^n$. We require that Ω be a smooth n-dimensional manifold with boundary. The boundary of Ω will be denoted $\partial\Omega$. The compactness of Ω means that it is a closed and bounded set of $\mathbb{R}^n$. The fact that Ω is a manifold with boundary ensures that $\partial\Omega$ is a smooth, non-intersecting manifold that separates $\mathbb{R}^n$ into a distinct interior and exterior. These properties are designed to capture the essence of what it means for an object to be solid. As an example, Ω could be the closed unit ball $\overline{B^n} = \{x \in \mathbb{R}^n \mid \|x\| \leq 1\}$. The boundary of the $\overline{B^n}$ is the unit sphere, i.e., $\partial\overline{B^n} = S^{n-1} = \{x \in \mathbb{R}^n \mid \|x\| = 1\}$.

We define a *solid object* to be an embedding of $\partial\Omega$ into $\mathbb{R}^n$ (Fig. 1). Recall that a mapping $f : \partial\Omega \to \mathbb{R}^n$ is an embedding if it is a diffeomorphism of $\partial\Omega$ onto its image $f(\partial\Omega)$. The space of all such embeddings forms an infinite-dimensional manifold, which is denoted $\mathcal{E}(\partial\Omega, \mathbb{R}^n)$. Since each object f is defined to be an embedding of $\partial\Omega$, the image $f(\partial\Omega)$ is also a smooth, non-intersecting compact manifold that separate $\mathbb{R}^n$ into a distinct interior and exterior. In other words, f preserves our notion of what it means to be solid. Notice that the choice of Ω will determine a fixed topology for the possible objects in the space. However, if Ω and Ω' are two diffeomorphic template objects, then the resulting object spaces $\mathcal{E}(\partial\Omega, \mathbb{R}^n)$ and $\mathcal{E}(\partial\Omega', \mathbb{R}^n)$ are equivalent. In other words, the definition of our object space is independent of the template object up to diffeomorphism.

A path in $\mathcal{E}(\partial\Omega, \mathbb{R}^n)$ is a one-parameter family of embeddings, $c : (a, b) \times \partial\Omega \to \mathbb{R}^n$ (Fig. 1). For each real number $t \in (a, b)$, the point $c(t) \in \mathcal{E}(\partial\Omega, \mathbb{R}^n)$

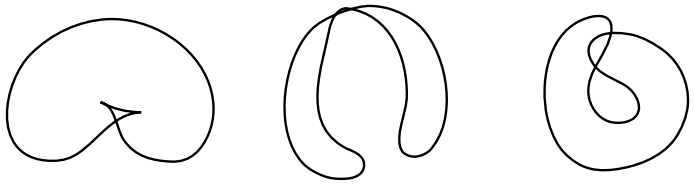

Fig. 2. The possible forms of self-intersections of an object's boundary: local singularity (left), global interior crossing (middle), and global exterior crossing (right).

is an object, and the path c is a smooth deformation of objects parameterized by t. For each $x \in \partial\Omega$ the path c generates a curve in $\mathbb{R}^n$: $t \mapsto c(t)(x)$. The t derivative of this curve, $c_t(t)(x)$, is a vector in $T_{c(t)(x)}\mathbb{R}^n$, the tangent space of $\mathbb{R}^n$ at the point $c(t)(x)$. Thus, the tangent vector $c_t(t)$ is a mapping that assigns to each $x \in \partial\Omega$ the vector $c_t(t)(x) \in T_{c(t)(x)}\mathbb{R}^n$ (Fig. 1). Intuitively, the tangent vector $c_t(t)$ can be thought of as an infinitesimal deformation of the object $c(t)$. The space of all tangent vectors to an object $f \in \mathcal{E}(\partial\Omega, \mathbb{R}^n)$ forms the vector space $T_f\mathcal{E}(\partial\Omega, \mathbb{R}^n) = C^\infty(\partial\Omega, f^*T\Omega_f)$, where f^* denotes the pull-back via f, and $\Omega_f = f(\Omega)$ is the current shape.

Notice that the parameterization of the object boundary is included in our definition of a solid shape. This is in contrast to recent work on planar curves, e.g., [9], [10], [11], where shape is defined modulo reparameterizations. Glaunes et al. [14] and Michor and Mumford [15] also show that metrics on the diffeomorphism group can be used to induce metrics on the space of unparameterized shapes, which they define as the quotient space $\mathit{Diff}(\mathbb{R}^n)/\mathit{Diff}(\mathbb{R}^n, S^{n-1})$, where $\mathit{Diff}(\mathbb{R}^n)$ is the space of diffeomorphisms on $\mathbb{R}^n$ and $\mathit{Diff}(\mathbb{R}^n, S^{n-1})$ are the diffeomorphisms that map the sphere S^{n-1} to itself. By including the parameterization of the boundary, our framework allows correspondences to be made between the boundaries of different objects. This is desirable in medical image applications, where it is typically necessary that corresponding anatomical features be compared across subjects.

3 Riemannian Metrics on $\mathcal{E}(\partial\Omega, \mathbb{R}^n)$

We now define a new class of Riemannian metrics on the space of solid objects, $\mathcal{E}(\partial\Omega, \mathbb{R}^n)$, that are particularly well-suited for solid shape analysis as they prevent self-intersections of shapes. A Riemannian metric on $\mathcal{E}(\partial\Omega, \mathbb{R}^n)$ assigns a smoothly-varying inner product on each tangent space $T_f\mathcal{E}(\partial\Omega, \mathbb{R}^n)$. We denote the inner product of two tangent vectors $v, w \in T_f\mathcal{E}(\partial\Omega, \mathbb{R}^n)$ by $\langle v, w\rangle_f$. The length of a tangent vector v is given by $\|v\|_f = \sqrt{\langle v, v\rangle_f}$. A geodesic is a path γ that minimizes the energy $E(\gamma) = \int_a^b \|\gamma_t(t)\|^2_{\gamma(t)}\, dt$.

3.1 Preventing Boundary Intersections

Intersections of the boundary result when the object mapping $f : \partial\Omega \to \mathbb{R}^n$ fails to be an embedding, that is, it falls outside of the space $\mathcal{E}(\partial\Omega, \mathbb{R}^n)$. There

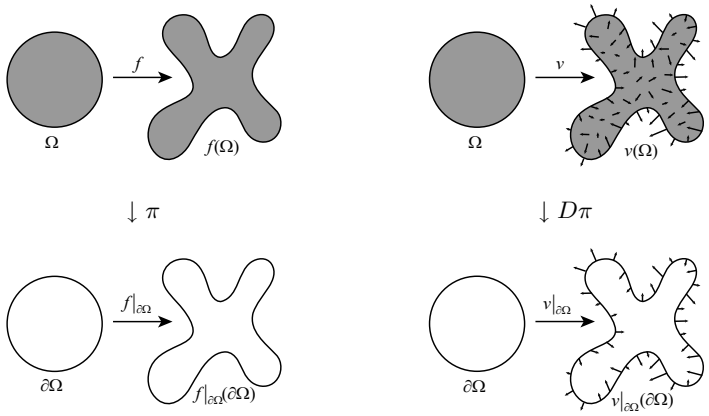

Fig. 3. Projection from the space of full embeddings to the space of boundary embeddings (left). Projection of a tangent vector (right).

are essentially three types of self-intersections of the object boundary that can occur (Fig. 2): local singularities, global interior crossings, and global exterior crossings. Local singularities happen when the derivatives of the object mapping become singular. Global interior crossings occur when the interior of the object collapses and the boundary touches itself. Global exterior crossings occur when the object boundary penetrates itself from the outside. Notice that the local singularities can be detected using only local information of the boundary, i.e., derivatives. However, the boundary of an object with a global intersection may still be smooth, and there is no way to detect these crossings with local information. In the next section we define a Riemannian metric on $\mathcal{E}(\partial\Omega, \mathbb{R}^n)$ that is capable of preventing local singularities and global interior crossings by involving the interior of the object. The exterior global crossings, which are not prevented in our framework, present a unique difficulty in that they involve events that happen external to the object.

3.2 Metrics via Projection

If we are to keep objects from collapsing, it is only natural that velocities of interior points in the object should play a role in the metric. The challenge is to accomplish this while defining a metric that is determined uniquely by the boundary velocities. We do this by defining a metric on the space $\mathcal{E}(\Omega, \mathbb{R}^n)$ of embeddings of Ω in such a way that a vector field on the boundary of the object can be extended to a vector field on the interior with minimal norm. This will allow us to compute geodesics in $\mathcal{E}(\Omega, \mathbb{R}^n)$ that take into account the interior of the object, and then project them back down to geodesics on the solid object space $\mathcal{E}(\partial\Omega, \mathbb{R}^n)$.

There is a natural projection $\pi : \mathcal{E}(\Omega, \mathbb{R}^n) \to \mathcal{E}(\partial\Omega, \mathbb{R}^n)$ given by the restriction to $\partial\Omega$. That is, for an embedding $f \in \mathcal{E}(\Omega, \mathbb{R}^n)$, we have $\pi(f) = f|_{\partial\Omega}$. The

derivative map of this projection, $D\pi : T\mathcal{E}(\Omega, \mathbb{R}^n) \rightarrow \mathcal{E}(\partial\Omega, \mathbb{R}^n)$, is also given by a restriction. Given a tangent vector $v \in T_f\mathcal{E}(\Omega, \mathbb{R}^n)$, we have $D\pi(v) = v|_{\partial\Omega}$. These projections are illustrated in Fig. 3. We define a metric on $\mathcal{E}(\Omega, \mathbb{R}^n)$ such that the projection π induces a unique metric on the space $\mathcal{E}(\partial\Omega, \mathbb{R}^n)$.

If $f \in \mathcal{E}(\Omega, \mathbb{R}^n)$ is an embedding, then at each point $x \in \Omega$ the Jacobian matrix $Df(x)$ has positive determinant. Thus, $Df(x)$ is an element of $GL^+(n, \mathbb{R})$, the Lie group of all positive-determinant matrices. We now define the metric on $\mathcal{E}(\Omega, \mathbb{R}^n)$ at the point f as

$$\langle v, w \rangle_f = \int_\Omega \langle Dv, Dw \rangle_{Df} \, dx, \tag{1}$$

where the inner product inside the integral is a right-invariant Lie group metric on $GL^+(n, \mathbb{R})$. There are several possible right-invariant metrics on $GL^+(n, \mathbb{R})$, which lead to an entire class of metrics on $\mathcal{E}(\Omega, \mathbb{R}^n)$ of the form (1). In this paper we use the metric

$$\langle Dv, Dw \rangle_{Df} = \operatorname{tr}\left(DvDf^{-1} \left(DwDf^{-1} \right)^T \right). \tag{2}$$

Notice that the value of (2) approaches infinity if Df approaches a zero determinant matrix. This property of the metric means that geodesic paths generate shape mappings with positive Jacobians, and thus do not generate local singularities or interior self-intersections.

We now use the metric (1) on $\mathcal{E}(\Omega, \mathbb{R}^n)$ and the projection mapping π to induce a metric on the solid object space $\mathcal{E}(\partial\Omega, \mathbb{R}^n)$. Given a tangent vector $v \in T_f\mathcal{E}(\partial\Omega, \mathbb{R}^n)$, we define an extension of v to the interior of Ω. An extension of v is a tangent vector $\tilde{v} \in T_{\tilde{f}}\mathcal{E}(\Omega, \mathbb{R}^n)$ such that $\pi(\tilde{f}) = f$ and $D\pi(\tilde{v}) = v$. The vector $\tilde{v}$ is chosen as the extension of v with minimal length in the metric (1), that is, $\tilde{v}$ is an extremal of the norm

$$\|\tilde{v}\|_{\tilde{f}} = \int_\Omega \operatorname{tr}\left(D\tilde{v} A D\tilde{v}^T \right) dx, \qquad A = D\tilde{f}^{-1} D\tilde{f}^{-1T}. \tag{3}$$

This is a variational problem that leads to the Euler-Lagrange equation

$$\operatorname{div}(A \nabla \tilde{v}) = 0. \tag{4}$$

This equation is an elliptic PDE since the matrix A is symmetric, positive-definite. The constraint that $\tilde{v}|_{\partial\Omega} = v$ provides the boundary conditions. Since it is an elliptic PDE with smooth boundary conditions, it has a unique solution. In other words, the vector v lifts to a unique vector $\tilde{v}$ with minimal norm. Therefore, we can define the metric on $\mathcal{E}(\partial\Omega, \mathbb{R}^n)$ to be $\langle v, w \rangle_f = \langle \tilde{v}, \tilde{w} \rangle_{\tilde{f}}$.

The metric defined in (1) is dependent on the choice of the template object Ω and the mapping f from that template to the current shape. This dependence can be removed by including the Jacobian of f in the integral to give the metric

$$\langle v, w \rangle = \int_\Omega \langle Dv, Dw \rangle_{Df} |Df| dx,$$

where $|Df|$ denotes the absolute value of the determinant of Df. This metric is right-invariant, meaning that it is left unchanged by a diffeomorphism of Ω. In other words, the metric is independent of the choice of the mapping f or of the choice of Ω, up to a diffeomorphism. Another possibility is to keep the metric (1), but restrict to only volume-preserving maps, i.e., $|Df| = 1$. A right-invariant metric also has the desirable property that the projection mapping π becomes a Riemannian submersion [16]. This has the consequence that any geodesic γ in the space $\mathcal{E}(\Omega, \mathbb{R}^n)$ has projection $\pi(\gamma)$ that is also a geodesic in $\mathcal{E}(\partial\Omega, \mathbb{R}^n)$. In this paper we focus on the metric given in (1), while the preferred right-invariant metrics are a current area of research.

4 Computing Geodesics

In this section we describe how to compute geodesics in $\mathcal{E}(\partial\Omega, \mathbb{R}^n)$ equipped with the metric induced by (1). We lift the geodesic computations to the space $\mathcal{E}(\Omega, \mathbb{R}^n)$ and then project these geodesics back to $\mathcal{E}(\partial\Omega, \mathbb{R}^n)$ via the mapping π. A geodesic path γ on $\mathcal{E}(\Omega, \mathbb{R}^n)$ is an extremal of the energy functional $E(\gamma) = \int_a^b \int_\Omega \|D\gamma_t\|^2_{D\gamma}\ dx\ dt$, where the metric is defined as in (1), and we are given initial conditions $\gamma(0)|_{\partial\Omega} = f_0$ and $\gamma_t(0)|_{\partial\Omega} = v_0$. The first step is to lift these initial conditions to extensions $\tilde{f}_0$ and $\tilde{v_0}$ defined on all of Ω. Any extension of f_0 may be chosen, and the extension of v_0 is computed via (4).

4.1 Geodesics of Matrix Fields

Rather than solve the above variational problem directly for γ, we instead solve for the Jacobian matrix $D\gamma$. Then, at each time point t, we integrate $D\gamma(t)$ with respect to the spatial variable x to arrive at the final geodesic γ. Consider a time-varying matrix field, $M : (a, b) \times \Omega \to GL(n, \mathbb{R})$, which represents the Jacobian field for the geodesic γ, i.e., $M = D\gamma$. The energy functional now becomes

$$E(M) = \int_a^b \int_\Omega \|M_t\|^2_M\ dx\ dt, \tag{5}$$

with initial conditions $M(0) = Df_0$ and $M_t(0) = Dv_0$. However, solving for extremals M of the energy (5) is not equivalent to solving for extremals $D\gamma$ of the energy $E(\gamma)$. To make them equivalent, M must be constrained to be the Jacobian field of a mapping, that is, M must be kept integrable. The integrability condition is $\text{curl}(M) = 0$, where we define the curl of a matrix field as the component-wise curl of each of its row vectors.[1]

If we first consider the unconstrained variational problem in (5), the extremals are given by pointwise geodesics on $GL^+(n, \mathbb{R})$, that is, for each $x \in \Omega$ the curve $t \mapsto M(t)(x)$ is a geodesic on $GL^+(n, \mathbb{R})$ under the right-invariant

[1] For our purposes the curl of a 2D vector field v is the scalar field $\text{curl}(v) = \partial v_2/\partial x - \partial v_1/\partial y$. The curl of a 3D vector field v is the vector field $\text{curl}(v) = \nabla \times v$.

metric. These geodesics can be computed as the following system of first-order ODEs (see [17] and also [18] p. 277)

$$M_t = XM, \tag{6}$$

$$X_t = XX^T - X^TX, \tag{7}$$

where the initial conditions are given in the form $M(0) = M_0$ and $X(0) = X_0$. Actually, there is a closed-form solution to these equations. It is given by

$$M(t) = \exp(t(X_0 + X_0^T)) \exp(-tX_0^T)M_0. \tag{8}$$

Notice that if M is constant in x, that is, if the shape deformation is an affine transformation, then the integrability constraint is satisfied automatically. This results in an important property of this metric: affine transformations of objects can be computed as closed form geodesics using (8).

4.2 Projection

We now describe the projection step used to solve the integrability constraint . We only consider the 2D case here, although the 3D case is similar. We are given a matrix field M_t, and we want to project it onto the space of integrable matrix fields on Ω, denoted $I(\Omega)$. Again, a matrix field X is in $I(\Omega)$ if $\mathrm{curl}(X) = 0$. The projection needs to be orthogonal under the metric (1). The orthogonal subspace to $I(\Omega)$ under this metric, denoted $I^{\perp}(\Omega)$, consists of all matrix fields of the form $DwJA^{-1}$, where w is a smooth vector field, $J = \begin{pmatrix} 0 & -1 \\ 1 & 0 \end{pmatrix}$, and A is given in (3). This is similar to the Helmholtz decomposition of a vector field into curl-free and divergence-free components. The difference is that the Helmholtz decomposition is orthogonal under the L^2 metric.

We now formulate the projection as a variational problem. Given a matrix field X that we want to project to $I(\Omega)$, we find the nearest matrix field in $I^{\perp}(\Omega)$ and subtract it from X. This is given by the matrix field $DwJA^{-1}$, where w minimizes the energy $E(w) = \int_{\Omega} \|DwJA^{-1} - X\|_{Df}^2 \, dx$. An extremal for this energy satisfies the Euler-Lagrange equation

$$\mathrm{div}\left(JA^{-1}J^TDw^T\right) = \mathrm{div}\left(JX^T\right). \tag{9}$$

This is a second-order elliptic PDE, and the orthogonality dictates that Dirichlet boundary conditions should be used. We solve this equation using a successive over-relaxation (SOR) method [19].

5 Results

In this section we give examples of the geodesic paths in the space of 2D solid objects, using the framework developed in this paper. To illustrate the power of our approach to prevent self-intersections, we compare our results to minimal

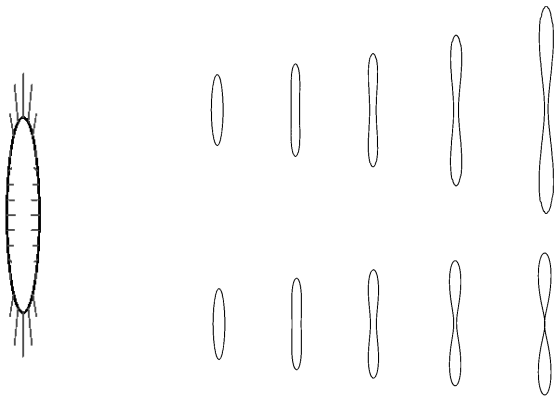

Fig. 4. Minimal paths of the pinching deformation for both the solid metric (top right) and the L^2 metric (bottom right). The initial velocity for both is shown on the left.

paths under a linear metric, i.e., the L^2 metric. The starting object for each example was an ellipse defined as $c(\theta) = ((1/6)\cos\theta, \sin\theta)$. This object was embedded in a uniformly-spaced 50×300 grid. The geodesic equations (6)-(7) were solved on a fixed grid using a second-order Runge-Kutta method [19].In each example we give an initial velocity vector on the boundary of the ellipse as the initial condition to the geodesic problem.

We first give an example of an affine transformation for which the solid shape geodesics can be computed in closed form using (8). The deformation is a stretching along the y-axis. The initial velocity vector (u, v) is given by $u(x, y) = -x, \quad v(x, y) = y$. The geodesic for the solid object metric is given by a path of embeddings $\gamma(t)(x) = M(t)x$, where M is the diagonal matrix with diagonal entries $\{e^{-t}, e^{t}\}$. It is clear that the matrix M has positive determinant for all t, and thus produces only valid, non-intersecting objects. In contrast, the minimal path under the L^2 metric for the same initial conditions is given by $c(t)(\theta) = ((1-t)(1/6)\cos\theta, (1+t)\sin\theta)$. This results in the ellipse collapsing to a vertical line at $t = 1$.

The second example is a pinch deformation (Fig. 4). The initial velocity vector (u, v) is given by $u(x, y) = -x^3 + 3xy^2 - x, \quad v(x, y) = -3x^2y + y^3$. The geodesic from the solid object metric nicely prevents the interior of the object from collapsing. Much like in the stretching example, the boundary slows down the closer it gets to itself. Under the L^2 metric the pinch eventually collapses into an interior global crossing.

The final example is a bending deformation (Fig. 5). The initial velocity vector (u, v) is given by $u(x, y) = (5/4)(x^2 - y^2) - x, \quad v(x, y) = (5/4)xy - y$. The resulting geodesic under the solid object metric produces qualitatively what we expect from a bending deformation. The minimal path under the L^2 metric starts out like a bending, but eventually begins to cross itself. This example shows how nonlinear deformations such as bending are not readily captured by

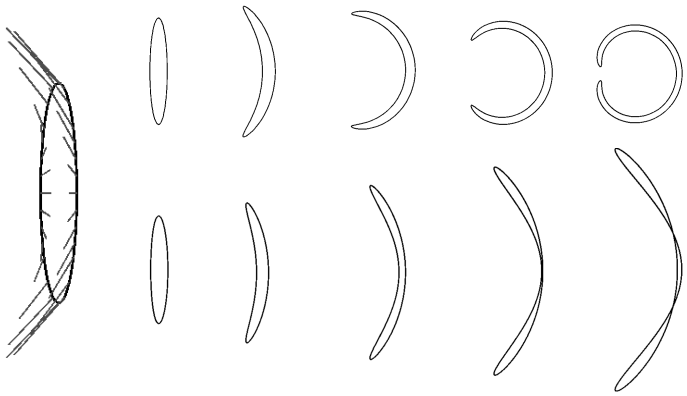

Fig. 5. Minimal paths of the bending deformation for both the solid metric (top right) and the L^2 metric (bottom right). The initial velocity for both is shown on the left.

linear metrics. The geodesics developed in this paper, on the other hand, are able to naturally model such nonlinear deformations.

6 Conclusion

We presented a new framework for shape analysis that directly models solid objects. Our method is based on representing the space of solid objects as an infinite-dimensional Riemannian manifold. We showed that the formulated metric possesses several desirable properties, including that it is valid for representing both 2D and 3D objects and that it can prevent certain types of self-intersections of object boundaries. We intend to pursue the use of this shape metric as a basis for statistical analysis of shape in computer vision and medical image analysis applications.

Acknowledgements

This work is part of the National Alliance for Medical Image Computing (NAMIC), funded by the National Institutes of Health through the NIH Roadmap for Medical Research, Grant U54 EB005149. Information on the National Centers for Biomedical Computing can be obtained from `http://nihroadmap.nih.gov/bioinformatics`.

References

1. Kendall, D.G.: Shape manifolds, Procrustean metrics, and complex projective spaces. Bulletin of the London Mathematical Society **16** (1984) 18–121

2. Bookstein, F.L.: Size and shape spaces for landmark data in two dimensions (with discussion). Statistical Science **1** (1986) 181–242
3. Mardia, K.V., Dryden, I.L.: Shape distributions for landmark data. Advances in Applied Probability **21** (1989) 742–755
4. Dryden, I., Mardia, K.: Statistical Shape Analysis. John Wiley and Sons (1998)
5. Small, C.G.: The statistical theory of shape. Springer (1996)
6. Cootes, T.F., Taylor, C.J., Cooper, D.H., Graham, J.: Active shape models – their training and application. Comp. Vision and Image Understanding **61** (1995) 38–59
7. Kelemen, A., Székely, G., Gerig, G.: Elastic model-based segmentation of 3-D neuroradiological data sets. IEEE Trans. on Medical Imaging **18** (1999) 828–839
8. Fletcher, P.T., Lu, C., Joshi, S.: Statistics of shape via principal geodesic analysis on Lie groups. In: Proceedings of the IEEE Conference on Computer Vision and Pattern Recognition (CVPR). (2003) 95–101
9. Klassen, E., Srivastava, A., Mio, W., Joshi, S.H.: Analysis of planar shapes using geodesic paths on shape spaces. IEEE Transactions on Pattern Analysis and Machine Intelligence (2003) 372–383
10. Sharon, E., Mumford, D.: 2d-shape analysis using conformal mapping. In: Proceedings of the IEEE Conference on Computer Vision and Pattern Recognition (CVPR). (2004) 350–357
11. Michor, P.W., Mumford, D.: Riemannian geometries on spaces of plane curves. (to appear Journal of the European Mathematical Society)
12. Grenander, U.: General Pattern Theory. Oxford University Press (1993)
13. Miller, M.I., Younes, L.: Group actions, homeomorphisms, and matching: A general framework. International Journal of Computer Vision **41** (2001) 61–84
14. Glaunès, J., Trouvé, A., Younes, L.: Modeling planar shape variation via Hamiltonian flows of curves. (preprint: `http://cis.jhu.edu/~younes/Preprints/glaunes.curves.pdf`)
15. Michor, P.W., Mumford, D.: An overview of the Riemannian metrics on spaces of curves using the Hamiltonian approach. (preprint: `http://lanl.arxiv.org/PS_cache/math/pdf/0605/0605009.pdf`)
16. O'Neill, B.: The fundamental equations of a submersion. Michigan Mathematical Journal **13** (1966) 459–469
17. Wang, H.C.: Discrete nilpotent subgroups of Lie groups. Journal of Differential Geometry **3** (1969) 481–492
18. Helgason, S.: Differential Geometry, Lie Groups, and Symmetric Spaces. Academic Press (1978)
19. Press, W.H., Teukolsky, S.A., Vetterling, W.T., Flannery, B.P.: Numerical Recipes in C++: The Art of Scientific Computing. 2nd edn. Cambridge University Press (2002)